IEEE Access
Multidisciplinary | Rapid Review | Open Access Journal

Received 2 July 2024, accepted 21 July 2024, date of publication 25 July 2024, date of current version 12 September 2024.

Digital Object Identifier 10.1109/ACCESS.2024.3433452

RESEARCH ARTICLE

Optimization on Torque Ripple Performance in ISG Motors With Fractional Slot Distributed Windings and Rotor Notching

YUNFEI DAI[1,2], DONG-WOO LEE[1], (Member, IEEE), HOUNG-KUN JOUNG[1], AND HO-JOON LEE[1], (Member, IEEE)

[1]Department of Electrical and Control Engineering, Cheongju University, Cheongju 28503, South Korea
[2]College of Physics and Electronic Engineering, Xinyang Normal University, Xinyang 464000, China

Corresponding author: Ho-Joon Lee (hjlee@cju.ac.kr)

This work was supported in part by the Korea Institute for Advancement of Technology (KIAT) grant funded by the Ministry of Trade, Industry & Energy (MOTIE) of Korea under Grant P0020536 as part of the Human Resource Development (HRD) Program for Industrial Innovation, and in part by the Basic Science Research Program through the National Research Foundation of Korea (NRF) funded by the Ministry of Education under Grant NRF-2020R1I1A3069569.

ABSTRACT The torque ripple of an electrical machine will affect the control accuracy and trigger vibration and noise in the system. Consider only the motor itself, the torque ripple is mainly caused by the cogging torque at no load, the harmonic component of the induced electromotive force, and the saturation of the magnetic fields in load operation. In this paper, a two-stage optimization approach is used to reduce torque ripple and cogging torque for an integrated starter and generator(ISG) machine. The first level of optimization mainly adopts the appropriate pole-slot combinations, and for a machine with an initial model of 6-pole/36-slot, it is optimized to 8-pole/36-slot, which significantly reduces the cogging torque and torque ripple. The second level of optimization is rotor notching, and the notch strategy is classified into three types, Q-axis notch, magnetic bridge notch(MB notch), and Q-axis and magnetic bridge notch combination(QMC notch), and the selection of each notching parameters is analyzed respectively. For the Q-axis notch, the parameter sweep method is mainly used to determine the parameters, and for MB notch and QMC notch, the non-dominated sorting genetic algorithm-II(NSGA-II) is used for multi-objective optimization to determine the parameters. Then torque performance and total harmonic distortion(THD) are analyzed for each design. Finally, the rotor strength was analyzed. Simulation results show that suitable pole-slot combinations can reduce the cogging torque and torque ripple to a greater extent. Selection of suitable rotor notching can improve the torque performance again to some extent, in which the QMC notch design is preferred and recommended.

INDEX TERMS Cogging torque, interior permanent magnet synchronous motor (IPMSM), notch, non-dominated sorting genetic algorithm-II (NSGA-II), torque ripple.

I. INTRODUCTION

Internal combustion engines (ICEs) have dominated the transportation sector for decades, but their energy sources depletion coupled with the hazardous emissions has pushed the world to move away from fossil-fuels based transportation sector [1]. Manufacturers, governments, and consumers increasingly gravitate towards electric (EVs) and hybrid electric vehicles (HEVs) to address these concerns [2]. For HEVs, they are classified as micro HEVs, mild HEVs, and full HEVs depending on the operating voltage and electrical power level [3]. In a micro HEVs system, the starter and the generator are integrated into a single electric machine called integrated starter and generator(ISG), which serves the dual purpose of starting and generating electricity [4]. As one type of ISG, the belt-driven ISG is widely used because of its

The associate editor coordinating the review of this manuscript and approving it for publication was Jorge Esteban Rodas Benítez.

ability to be installed in existing generator locations and its excellent performance in terms of overall vehicle cost control and technical feasibility [5].

Permanent magnet (PM) ISG motors are required to provide high starting torque during cold engine startup and to produce high electric power in the idle-to-maximum speed range of the engine, which requires good flux-weakening ability. The interior permanent magnet synchronous motor (IPMSM) is one of the most attractive ISG motors due to its excellent flux-weakening ability [6]. An important factor affecting the performance of IPMSM is the rotor topology structure. Therefore, determining an appropriate IPMSM rotor topology structure is essential for designing a motor for electrical vehicles (EVs) [7]. ISG motors usually have a V-shape or a Bar-shape topology for the rotor. Although the V-shape rotor structure has a larger camber ratio to increase the reluctance torque, the Bar-shape rotor has better power characteristics for power generation operation.

However, the IPMSM has a sensitivity of design related to vibration due to the torque ripple and cogging torque. Therefore, reducing the torque ripple and cogging torque becomes an increasingly critical issue in the IPMSM design. Current research has proposed a variety of motor design and optimization methods for reducing torque ripple and cogging torque. For IPMSM, consider only the motor body design, the main methods contain three categories, the first one of which is to adopt different combinations of slot-pole, the second one of which is to optimize the winding type of the stator and the third one of which is to optimize the stator-rotor or permanent magnet geometry [8]. In [9], a space-shifted wye-delta stator winding is used to minimize torque ripple and radial force. In [10], The performance of single-V, double-V, and triangular magnet topologies in 48/8 and 36/8 integer-slot and fractional-slot IPMSM is compared, and it is found that the 36/8 fractional-slot configuration improves the torque quality at both low and high speed points. Jang et al. [11] studied the use of 12-pole 18-slot fractional slot windings to minimize torque ripple in HEV motors. The torque ripple characteristics of three rotor topologies, bar-shape, U-shape, and V-shape are analyzed. For the rotor, the reduction of torque ripple is by optimization of the barrier shape; for the stator, a wedge shape is applied to the stator shoe part to reduce the torque ripple. In [12], a piecewise inverse cosine function was used to modify the rotor shape to reduce torque ripple and electromagnetic noise. Moon and Kang [13] used an asymmetric shoe of stator and notch in stator is to reduce torque ripple and cogging torque. OCAK and AYDIN [14] proposed an innovative magnet-step-skew to minimize cogging torque and torque ripple. Peng et al. [15] proposed a rotor structure consisting of two segments staggered mechanically 180°. In each segment, the intersection angle between two magnets of one V-shaped pole is different from the others. This design mitigates torque ripple and electromagnetic vibration. Dai et al. [16] proposed a new method called reluctance harmonic configuration (RHC) to reduce torque ripple, this method can be applied to IPMSMs by making a simple adjustment to the rotor surface. Reference [17] proposed an optimal design method of IPMSM based on multi-objective optimization including the mechanical stress for high-speed EVs. That method is a sequential multi-physics handling method that consists of a two-step optimal process. Reference [18] used two rotor shapes, inverse-cosine-shaped (ICS) and ICS + third-harmonic-shaped (ICTHS) to reduce torque ripple and radial force harmonics.

The notched rotor design is increasingly used to reduce torque ripple and cogging torque [19]. In [20], Hwang et al. compared torque ripple and cogging torque with five different rotor notches, however, the researchers just selected only five locations, which was not comprehensive enough, and it is the same design of the experiment (DoE) problem in [21]. Sun and Tian [22] give the specific numerical design of a fractional-slot concentrated-winding(FSCW) IPMSM motor applying a rotor notch. However, the researchers used a proxy model of torque performance, which is inherently in error with the real motor model due to the nonlinearity of the problem. General Motors's He et al. [23] discussed the optimization of motor NVH by Q-axis notching and D-axis notching of the motor. Rotor notch selected from 4000 DoE runs is highly effective to reduce the dominant 96^{th} torque ripple order, and the optimal design is successfully implemented in the electric motor for General Motors Ultium electric drive units.

In this article, the theoretical analysis of the cogging torque and torque ripple of the IPMSM motor is carried out to obtain the expressions of the motor torque and cogging torque, respectively, and based on the analysis of the expressions, a two-stage optimization strategy is formulated to consider the trade-off relationship between the cogging torque and torque ripple. The first level of optimization is to reduce the cogging torque and torque ripple by adopting more appropriate pole-slot combinations, specifically with a fractional-slot distribution-winding (FSDW) design. The second level of optimization is rotor notching, and three types of notching designed are proposed.

The main innovations of this research work are, firstly, the comparison of three types of notched designs using a comprehensive DoE approach, and the application of the non-dominated sorting genetic algorithm-II (NSGA-II) optimization algorithm to quickly identify the optimal design variables. Secondly, the study employs a real-time interactive optimization approach instead of relying on an agent model of the motor, ensuring an error-free design.

II. ANALYSIS OF TORQUE PERFORMANCE OF PMSM

The electromagnetic torque of a motor is generated by the interaction of two magnetic fields or by the current subjected to the magnetic field. For IPMSM, the electromagnetic torque is mainly composed of permanent magnet torque and

reluctance torque. The permanent magnet torque is generated by the interaction of the armature magnetic field formed by the windings with the magnetic field of the permanent magnets, and the reluctance torque is the torque caused by the difference between the rotor's d-axis and q-axis reluctance [24].

A. TORQUE RIPPLE

For a conservative system with no energy loss, the output torque of the motor can be derived from the principle of virtual work [25],

$$T = \left.\frac{\partial W'_{\mathrm{m}}}{\partial \alpha_{\mathrm{m}}}\right|_{i=\mathrm{const}} = \sum_n i_n \frac{\partial \Psi_n}{\partial \alpha_{\mathrm{m}}} - \left.\frac{\partial W_{\mathrm{m}}}{\partial \alpha_{\mathrm{m}}}\right|_{i=\mathrm{const}} \quad (1)$$

where W'_{m} and W_{m} are magnetic energy and magnetic common energy of the system, i and Ψ are the current and magnetic chain, α_{m} is the mechanical angle of the motor, and n is the phase sequence of the winding.

For permanent magnet synchronous motors, the magnetic chain can be divided into the permanent magnet chain and the magnetic chain generated by the windings.

$$\Psi_n = \psi_n^{\mathrm{PM}} + \psi_n^i \quad (2)$$

where ψ_n^{PM} and ψ_n^i are permanent magnet chains and the magnetic chains that are generated by the windings. so the Eq. (1) can be written as

$$T = \sum_n i_n \frac{\partial \psi_n^{PM}}{\partial \alpha_m} + \sum_n i_n \frac{\partial \psi_n^i}{\partial \alpha_m} - \left.\frac{\partial W_m}{\partial \alpha_m}\right|_{i=\mathrm{const}} \quad (3)$$

In Eq. (3) the first item is the permanent magnet torque, and the second item is the reluctance torque. These two items are mainly generated because of electromagnetic factors, and the sum is the electromagnetic torque. It can be seen that the two components will rotate with the rotor, which means that they will produce a constant torque over time, but there will also be pulsating changes in torque. If interpreted in terms of Maxwell's tensor theory, the torque is generated by the tangential electromagnetic force. The fundamental magnetic field produced by the stator windings and the rotor magnetic field produces a constant torque. The harmonic magnetic field generated by the stator winding and the rotor magnetic field produces torque ripple.

The torque ripple studied in this research work are only those caused by the electromagnetic design of the motor body, and there are other causes of torque ripple, such as the harmonic currents introduced by the controller, the manufacturing errors of the motor, etc. [26], [27], which are beyond the scope of this research work.

Based on Eq. (3), the causes of torque ripple are classified into three categories as follows,

1) The cogging torque during no-load operation or when the torque is zero.
2) Harmonic components in the back-electromotive force(back-EMF).
3) The saturation of the magnetic fields due to load operation.

B. COGGING TORQUE

When the motor is running at no load, the permanent magnet torque and the reluctance torque are zero, and the third term is the cogging torque that changes with the rotor position, which can be expressed as [28]

$$T_{\mathrm{cog}} = -\left.\frac{\partial W_{\mathrm{m}}}{\partial \alpha_{\mathrm{m}}}\right|_{i=0} \quad (4)$$

Assuming that the permeability of the armature core is infinite, ignoring the effects of saturation, leakage, and cogging effects, and assuming that the permeability of the permanent magnets is the same as that of the air and that the stored energy of the magnetic field inside the motor is approximated to be the sum of the energy of the magnetic field in the motor's air-gap and the permanent magnets, the energy of the motor's internal magnetic field can be expressed as:

$$\begin{aligned} W_{\mathrm{m}} &= \frac{1}{2\mu_0}\int_V B^2(\theta, \alpha_{\mathrm{m}})\, dV \\ &= \frac{1}{2\mu_0}\int_V B_r^2(\theta)\, G^2(\theta, \alpha_{\mathrm{m}}) dV \\ &= \frac{1}{2\mu_0}\int_V B_r^2(\theta)\left[\frac{h_m(\theta)}{h_m(\theta)+\delta(\theta, \alpha_{\mathrm{m}})}\right]^2 dV \end{aligned} \quad (5)$$

where μ_0 is the permeability of vacuum, B is the air-gap magnetic density, θ is the angle along the rotor rotation direction, $B_r(\theta)$ is remanence of the permanent magnet, $G(\theta, \alpha_{\mathrm{m}})$ is relative air-gap permeance, $\delta(\theta, \alpha_{\mathrm{m}})$ is effective air-gap length at different positions along the circumference, $h_m(\theta)$ is the length of magnets in the magnetization direction.

According to the Fourier decomposition of $B_r^2(\theta)$ and $\{h_{\mathrm{m}}(\theta)/[h_{\mathrm{m}}(\theta)+\delta(\theta, \alpha_{\mathrm{m}})]\}^2$,

$$\begin{aligned} B_r^2(\theta) &= B_{r0} + \sum_{n=1}^{\infty} B_{rn}\cos 2np\theta \\ &= \alpha_p B_r^2 + \sum_{n=1}^{\infty}\frac{2}{n\pi}B_r^2 \sin n\alpha_p\pi \cos 2np\theta \end{aligned} \quad (6)$$

where B_{r0} is the constant terms of $B_r^2(\theta)$ after the Fourier decomposition, B_{rn} is the Fourier decomposition coefficient of remanence of the permanent magnet, α_p is the pole arc coefficient, p is the number of the pole pairs.

$$\left[\frac{h_m(\theta)}{h_m(\theta)+\delta(\theta, \alpha_{\mathrm{m}})}\right]^2 = G_0 + \sum_{n=1}^{\infty} G_n \cos nz(\theta + \alpha_{\mathrm{m}}) \quad (7)$$

where G_0 is the constant terms of $\{h_{\mathrm{m}}(\theta)/[h_{\mathrm{m}}(\theta) + \delta(\theta, \alpha_{\mathrm{m}})]\}^2$, G_n is the Fourier decomposition coefficient of the square of the relative air-gap permeability, and z is the number of the stator slots.

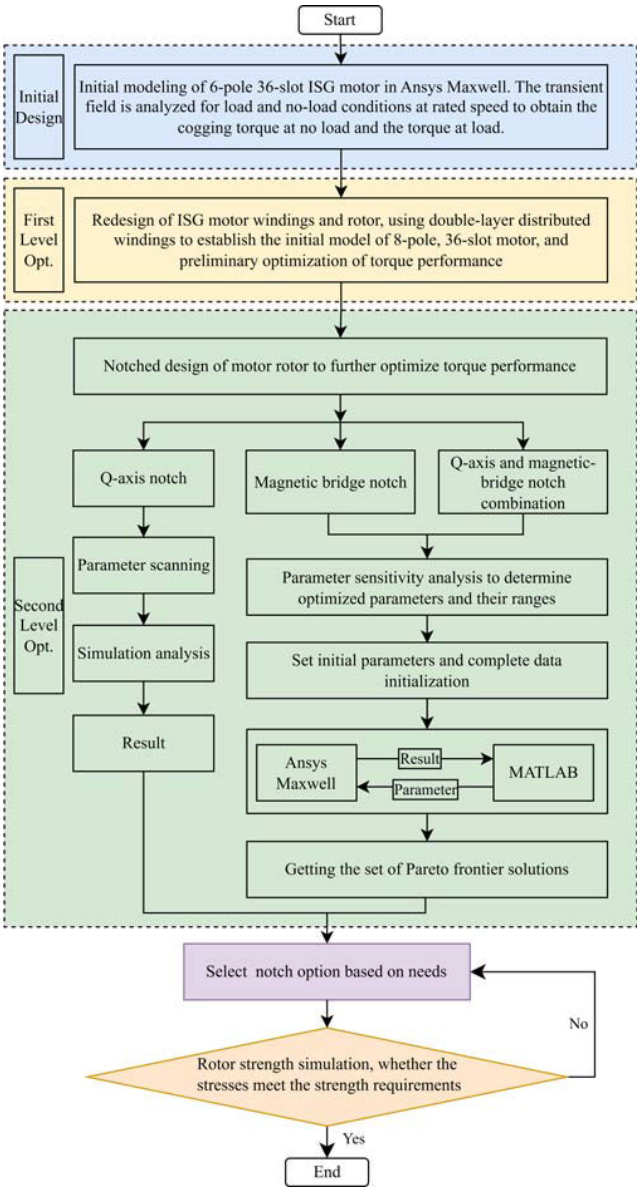

FIGURE 1. Flowchart of the design and optimization process.

Substituting equations (5), (6), and (7) into Eq. (4), the expression for the cogging torque of the motor is

$$T_{\mathrm{cog}}(\alpha_{\mathrm{m}}) = \frac{\pi z L_a}{4\mu_0}\left(R_2^2 - R_1^2\right)\sum_{n=1}^{\infty} nG_n B_{r\frac{nz}{2p}} \sin nz\alpha_{\mathrm{m}} \quad (8)$$

where L_a is the axial length of the armature core, and R_1 and R_2 are the outer radius of the armature and the inner radius of the stator yoke, respectively, n is the integer that makes $nz/2p$ an integer.

In this paper, the flowchart of design and optimization for torque performance is shown in Fig. (1). Section III initializes the design motor and introduces the specific parameters of the motor. Then, based on the analytical analysis of the cogging torque in Section II, a more suitable pole-slot combinations scheme is further discussed to reduce the cogging torque and torque ripple. Section IV based on the analytical analysis in Section II and the results of preliminary optimization in Section III, three types of rotor notching schemes are discussed to optimize the torque performance again, including Q-axis notch, notching near the magnetic bridge (MB notch), and Q-axis and magnetic bridge notch combination(QMC notch), and the experimental design of each type of rotor notching scheme is carried out and discussed. Among them, for Q-axis notch, because of fewer parameters, the best notching parameters are selected by scanning the parameters. MB notch and the QMC notch design involve too many parameters. The combination design will be more than one million if the method of sweeping parameters is used, so the sensitivity analysis of the parameters is carried out first. The parameters that have a greater impact on the torque performance are selected. The finite element analysis results are directly combined with the numerical optimization algorithms. The multi-objective optimization is realized by using NSGA-II, to obtain a Pareto solution set, which not only reduces the number of calculations and ensures the optimization efficiency, but also does not use the proxy model in the design optimization process, an error-free analysis design in turn being realized. At the end of this section, the torque performance of the four designs is compared and the no-load back-EMF as well as the air-gap radial flux density of the magnetostatic fields are analysed. In Section V, according to the actual needs, select the notch solutions based on needs, and verify the magnetic bridge strength of the rotor at the highest rotational speeds. Section VI is the conclusion of the paper.

III. MOTOR MODELING

A. INITIAL DESIGN OF THE ISG MOTOR

The initial ISG motor studied in this paper is a 6-pole, 36-slot IPMSM with a double winding layer and concentric winding type. Fig. 2a shows the cross-section of the initial ISG model. The outer stator yoke protrusion serves to secure the stator to the housing. The stator slot type is a parallel tooth. To better utilize the power characteristics of the motor, PMs are arranged in Bar-shape. To ensure that the strength of the rotor meets the requirements at high rotational speeds, the permanent magnet is divided into two pieces. Tab. 1 shows the main parameters of the model.

The motor is modeled in FEA software Ansys Maxwell and analyzed to obtain the cogging torque of the motor during no-load operation, and the torque during load operation at rate speed(4200r/min). In Fig. 3, the red curve is the cogging torque of the 6-pole/36-slot motor. The max value of cogging torque is 448.84 mNewtonMeter. In Fig. 4, the red curve is the torque of the 6-pole/36-slot motor. The average torque is 13.33 NewtonMeter. The peak-to-peak value of the output torque reached 3.9 NewtonMeter, which is huge for the ISG motor. The value of torque ripple can be expressed as,

$$T_{\mathrm{rip}} = \frac{T_{\max} - T_{\min}}{T_{\mathrm{avg}}} \times 100\% \quad (9)$$

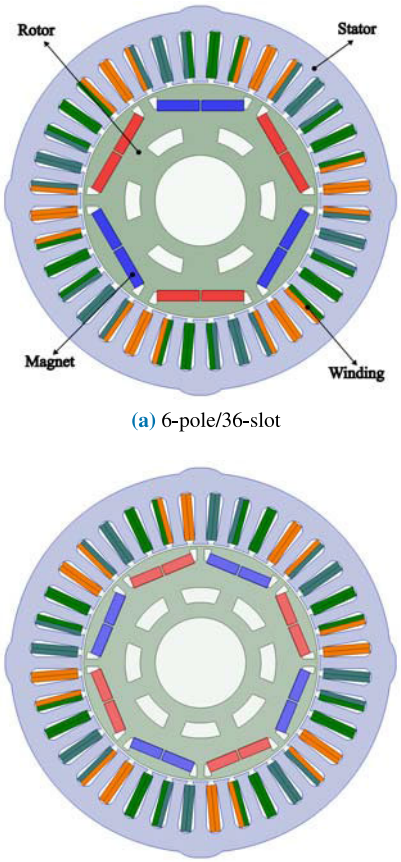

(a) 6-pole/36-slot

(b) 8-ploe/36-slot

FIGURE 2. The initial motor (6-pole/36-slot) and optimization model with suitable pole-slot combinations (8-pole/36-slot).

So, the T_{rip} of this ISG machine is 29.27%. The torque performance of the motor needs to be optimized. Optimization of pole-slot combinations is first considered to optimize torque performance.

B. OPTIMIZATION MODEL WITH SUITABLE POLE-SLOT COMBINATIONS

According to Eq. (8), the number of periods of the cogging torque is n

$$n = \frac{LCM(z, 2p)}{z} = \frac{2p}{GCD(z, 2p)} \tag{10}$$

where n is the number of periods of the cogging torque within a tooth pitch, $LCM(z, 2p)$ is the least common multiple between slot number and pole number, $GCD(z, 2p)$ is the greatest common divisor between slots number and poles number.

From Eq. (8), it can be seen that the maximum value of the cogging torque depends on the magnitude of $B_r \frac{nz}{2p}$. According to Eq. (6), the larger n is, that is to say, the larger the period number is, the smaller the corresponding $B_r \frac{nz}{2p}$ is. So, the use of a more appropriate pole-slot combination allows longer periods to reduce the cogging torque. The number of periods for a motor with 6 pole and 36 slot is 1, while the number of periods for a motor using 8 pole and 36 slot is 2. After optimization, the motor becomes a fractional slot and the windings are a double winding layer and distributed windings, as shown in Fig. (2b).In order not to change the magnet consumption, the initial model magnet consumption is $14.44mm \times 3.5mm \times 12$ and the optimized model magnet consumption is $10.83mm \times 3.5mm \times 16$, which is equal. Same area dimensions for stator and rotor and barriers.

As a comparison, the torque characteristics of an 8-pole/36-slot motor are modeled in Ansys Maxwell and

TABLE 1. Initial parameters of IPMSM.

Parameters	Value	Unit
Stator Outer Diameter	130	mm
Stator Inner Diameter	81.4	mm
Rotor Outer Diameter	80	mm
Rotor Inner Diameter	30.9375	mm
Air-gap	0.7	mm
Stack Length	78	mm
Rate Speed	4200	rpm
Max Speed	15000	rpm
PM Width	14.44	mm
PW Thickness	3.5	mm
Phase	3	
Permanent Magnet	N36Z	
Silicon Steel Sheet	50PN470	

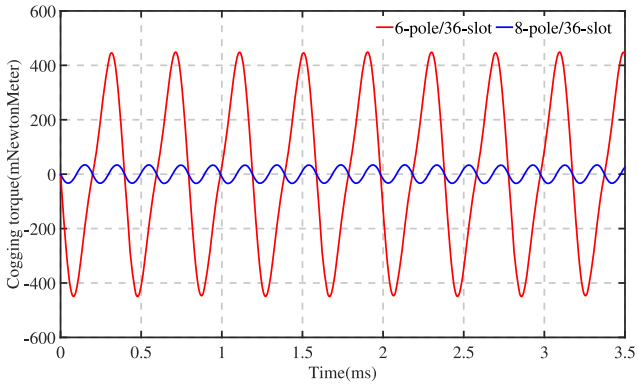

FIGURE 3. Cogging torque of 6-pole/36-slot and 8-pole/36-slot.

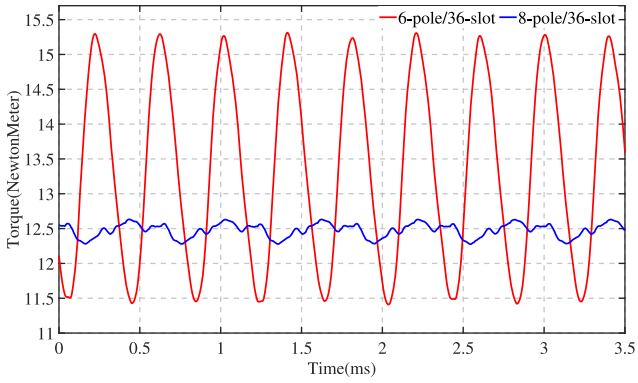

FIGURE 4. Torque of 6-pole/36-slot and 8-pole/36-slot.

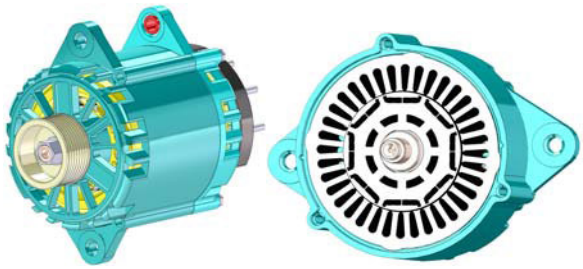

(a) Full model (b) Section-cross view

FIGURE 5. The 3D model of ISG motor.

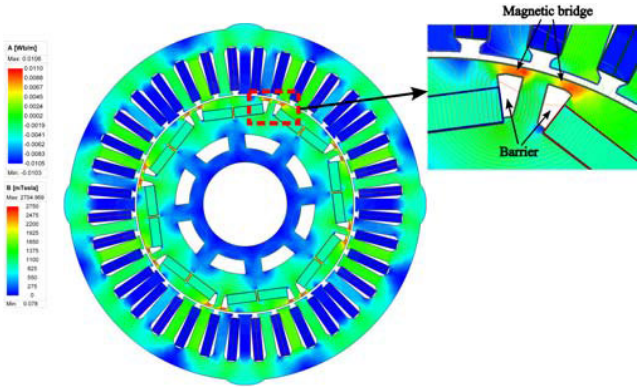

FIGURE 6. Magnetic field and flux line distribution of the ISG machine.

analyzed. In Fig. (3) and Fig. (4), the blue curve is the cogging torque and torque of 8-pole/36-slot motor. It can be seen that the cogging torque and torque ripple decrease by more than 10 times, which is a huge decrease. Although the average torque is reduced to 12.48N·m, it still meets the design requirement of an average torque greater than 11.4N·m.

Fig. (5) depicts the 3D model of the ISG motor, Fig. (5a) is the full model, and Fig. (5b) is the section-cross the 8-pole/36-slot ISG motor which depicts the stator and the rotor.

IV. OPTIMIZATION DESIGN OF ROTOR NOTCHED

Once the pole-slot combinations are determined, as seen in Eq. (8), it can be seen that the cogging torque can be reduced again by decreasing the amplitude of G_n. Therefore, the method of rotor notching is considered to reduce the magnitude of G_n. However, if the notch is inappropriately designed, it can change the magnetic field distribution during motor operation, resulting in a decrease in the average torque or greater torque ripple.

As can be seen from the magnetic field and line of magnetic force distribution diagram in Fig. (6), although the magnetic field saturation design of the magnetic bridge can isolate some of the magnetic flux leakage, there will still be magnetic flux leakage passing through. Not only that, but there are also magnetic flux leakage passing through the barriers on both sides(through the Q-axis). Therefore, notching can reduce magnetic flux leakage, and proper notching can also play a filtering role, which can filter some of the low harmonics, thus reducing torque ripple.

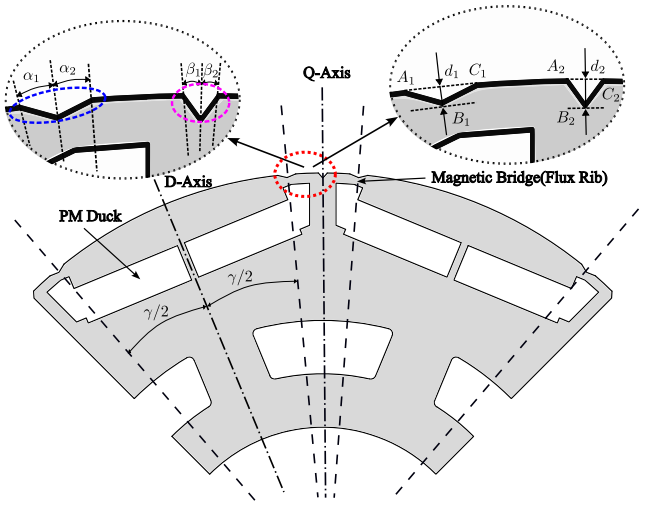

FIGURE 7. Rotor notching schematic.

Based on the above analysis and considering the magnetic field distribution, the notching design is categorized into three types, Q-axis notch, MB notch, and QMC notch. Three methods of notching are categorized and analyzed below. As shown in Fig. (7), the Q-axis notch is shown in the fuchsia dashed box, the MB notch is shown in the blue dashed box, and the red dashed box is the QMC notch.

A. Q-AXIS NOTCH

As shown in Fig. (7), the design parameters of the Q-axis notch, mainly include the notch depth d_2, the notch angles β_1 and β_2, and the fillet of each vertex (A_2, B_2, C_2) of the notch. The notch is designed as a symmetrical slot about the q-axis, that is, $\beta_1 = \beta_2$.

For the Q-axis notch, three parameters determine the design of the notch, notch angle, notch depth, and vertex fillet, according to the sensitivity analysis, the fillet has very little effect on the results, it can consider only two design parameters, the Q-axis notch offset angle β_2 and Q-axis notch depth d_2. When the rotor is running at the highest speed (15000rpm), it is necessary to ensure that the magnetic bridge strength meets the requirements, so the size of the notch should be controlled. Based on this, β_2 is set to $0.5° - 30°$ (Here's the electrical angle. All the following.) and d_2 is set to 0.1mm-0.5mm, as Tab. (2) shows.

Since the parameters as well as the range of values are small, the no-load cogging torque and load torque cases for all parameter combinations can be calculated by the sweep parameter method. By calculating three hundred design points, the swept parameter simulation results are analyzed and the appropriate parameter combinations are selected as Tab. (3) shows.

B. MAGNETIC BRIDGE NOTCH

As shown in Fig. (7), the MB notch is symmetric about the d-axis, and the angle with the d-axis is $\gamma/2$. The design parameters of the MB notch, include the MB notch offset

TABLE 2. Parameters range of notching.

Parameters	Q-axis notch	MB notch	QMC notch
$\gamma(^\circ)$	0	130-175	130-165
d_1(mm)	0	0.1-0.3	0.1-0.3
$\alpha_1(^\circ)$	0	0.5-25	0.5-25
$\alpha_2(^\circ)$	0	0.5-2.5	0.5-5
$\beta_2(^\circ)$	0.5-30	0	0.5-2.5
d_2(mm)	0.1-0.5	0	0.1-1

TABLE 3. Parameters value of notching.

Parameters	Q-axis notch	MB notch	QMC notch
$\gamma(^\circ)$	0	149	139
d_1(mm)	0	0.27	0.23
$\alpha_1(^\circ)$	0	20.665	18.065
$\alpha_2(^\circ)$	0	0.755	1.195
$\beta_2(^\circ)$	25	0	1.23
d_2(mm)	0.2	0	0.92

angle γ, notch depth d_1, the notch angles α_1 and α_2, and the fillet of each vertex (A_1, B_1, C_1) of the notch. Same as the Q-axis notch, the fillets of the vertices can be disregarded for now because they have little effect. So there are four parameters in MB notch design, MB notch offset angle γ, notch depth d_1, notch angles α_1, and notch angles α_2.

Considering that the electrical angle between the d-axis and the q-axis is 90 degrees, as well as the requirement of the magnetic bridge strength, the range of values of the four parameters is shown in Tab. (2).

If the same method of parameter sweeping is used to determine the parameter values, the design point reaches more than 30,000, which not only exceeds the range of software simulation, but also cost too much time, so the numerical method is considered to determine the parameter values. In order to minimize the motor cogging torque and torque ripple while the average torque meets the design requirements, the way to select the best parameters is a multi-objective global optimization problem [29].

Metaheuristic seems to be a generic algorithm framework or a black box optimizer that can be applied to almost all optimization problems [30]. NSGA-II is a multi-objective metaheuristic algorithm based on the natural process of evolution that we use to solve multi-objective global optimization problems. NSGA-II incorporates standard GA (select, crossover, and mutation) with non-dominated sorting and a new fitness value ''Crowding Distance''. Being faster, having a better sorting algorithm, it includes elitism which preserves an already founded Pareto optimal from deleting, and uses an explicit diversity preserving mechanism. Because of the above advantages of NSGA-II, NSGA-II is used in this paper to solve the multi-objective optimization problem [31].

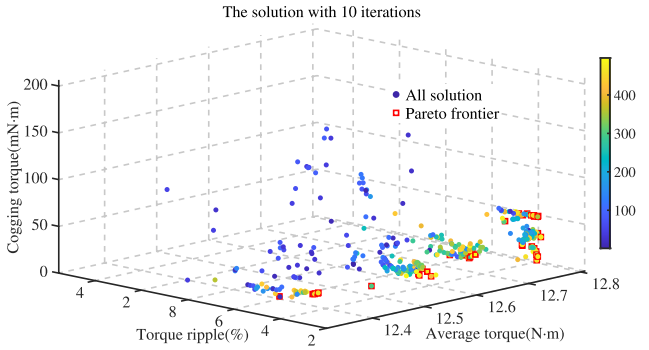

(a) MB notch

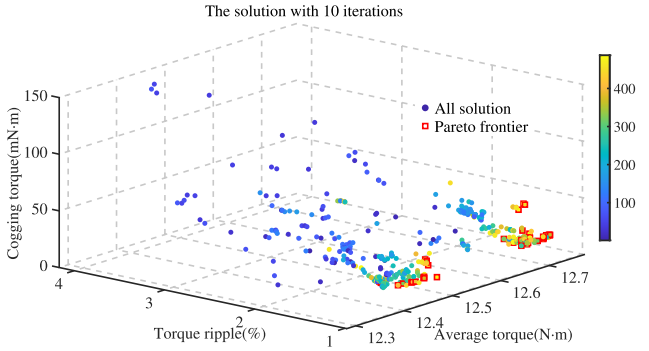

(b) QMC notch

FIGURE 8. MB notch and QMC notch multi-objective optimization results.

According to the above-mentioned, the optimization problem has four optimization parameters which are γ, d_1, α_1, and α_2. The optimization objectives are three, the torque ripple and the cogging torque are minimized and the average torque meets the requirements. In addition, it is also constrained by the range of values of the parameters and the strength of the rotor. The mathematical model is as follows,

$$\min : \begin{cases} f_1(x) = T_{\mathrm{cog}_{\max}} \\ f_2(x) = T_{\mathrm{rip}} \end{cases}$$

$$x = [\gamma, d_1, \alpha_1, \alpha_2]$$

$$\text{s.t.} \begin{cases} T_{\mathrm{avg}} \geqslant 11.4\ N \cdot m \\ \gamma + 2\alpha_2 \leqslant 180^\circ \\ 2\alpha_1 \leqslant \gamma \\ 0.1\ \mathrm{mm} \leqslant d_1 \leqslant 0.3\ \mathrm{mm} \end{cases}$$

Many researchers use the agent model for the optimization process, and in fact, the agent model has a large error with the actual model. Therefore, in this paper, by using MATLAB script file, and Ansys Maxwell real-time communication, to obtain the simulation results in Ansys Maxwell, the results of the data post-processing and optimization using the NSGA-II is carried out in MATLAB, and the optimized parameters are then returned to Ansys Maxwell, and subsequent iterative optimization processing, until the evolutionary iterative end.

Depending on the number of variables, a population size of 50 was chosen. The initial value of the crossover probability is set to 0.8. The initial value of the probability of variation

is set to 0.05. The number of evolutionary iterations is set to 10 generations. After 10 generations of evolution, 500 design points were obtained, as shown in Fig. (8a). The set of Pareto solutions can also be obtained, as shown by the small red box in Fig. (8a). From the set of solutions, the one with torque greater than the initial average torque and minimum torque ripple is selected as the optimal solution, as shown in Tab. (3).

C. Q-AXIS AND MAGNETIC BRIDGE COMBINED NOTCH

The combination of the above-mentioned Q-axis notch and MB notch is the QMC notch. Therefore, there are six design parameters, which are two design parameters in the Q-axis notch, β_2, and d_2, and four design parameters in the MB notch, γ, d_1, α_1, and α_2, respectively.

Similarly, if the parameter is determined using the sweep parameter method, the design points will reach more than one million depending on the step size of the range of the parameter, therefore, solving this multi-objective optimization problem still uses the NSGA-II real-time optimization method used in MB notch above to obtain the optimized parameters. The mathematical model is as follows,

$$\begin{aligned} \min: & \begin{cases} f_1(x) = T_{\mathrm{cog_{max}}} \\ f_2(x) = T_{\mathrm{rip}} \end{cases} \\ & x = [\gamma, d_1, \alpha_1, \alpha_2, \beta_2, d_2] \\ \text{s.t.} & \begin{cases} T_{\mathrm{avg}} \geqslant 11.4\, N \cdot m \\ \gamma + 2\alpha_2 + 2\beta_2 \leqslant 180^\circ \\ 2\alpha_1 \leqslant \gamma \\ 0.1\ \mathrm{mm} \leqslant d_1 \leqslant 0.3\ \mathrm{mm} \\ 0.1\ \mathrm{mm} \leqslant d_2 \leqslant 1\ \mathrm{mm} \end{cases} \end{aligned}$$

After 10 generations of evolution, 500 design points were obtained, as shown in Fig. (8b). The set of Pareto solutions can also be obtained, as shown by the small red box in Fig. (8b). From the set of solutions, the one with greater average torque than the initial design and minimum torque ripple is selected as the optimal solution, as shown in Tab. (3).

D. OPTIMIZATION RESULTS ANALYSIS

The design results of the three notching methods are simulated in Ansys Maxwell to obtain the no-load cogging torque curves, as shown in Fig. (9), and the load torque curves at the rated speed, as shown in Fig. (10), and the maximum value of the cogging torque and the average torque and torque ripple results of the four designs are listed in Tab. (4).

It can be seen that the cogging torque and torque ripple of the ISG motor can be reduced after the rotor notching optimization design. Among them, the most reduction in cogging torque is achieved by using a suitable Q-axis notch design, which is more than 10 times, and the most reduction in torque ripple is achieved by using a suitable QMC notch design, which is about 40%. For the average torque, all three designs can be greater than the average torque before the notching design, where the average torque is slightly increased by using the suitable MB notch design.

Based on Eq. (3), it is known that part of the torque ripple is due to the harmonic component of the back-EMF, which can be calculated using total harmonic distortion (THD), so it is necessary to analyze the back-EMF of several designs as well as calculate their THDs.

TABLE 4. Comparison of torque performance with different notch strategies.

	$T_{Cog_{max}}$(mN·m)	T_{Avg}(N·m)	T_{Rip}(%)
No notch	34.19	12.48	2.85
Q-axis notch	3.07	12.57	2
MB notch	16.90	12.86	2.52
QMC notch	10.72	12.58	1.71

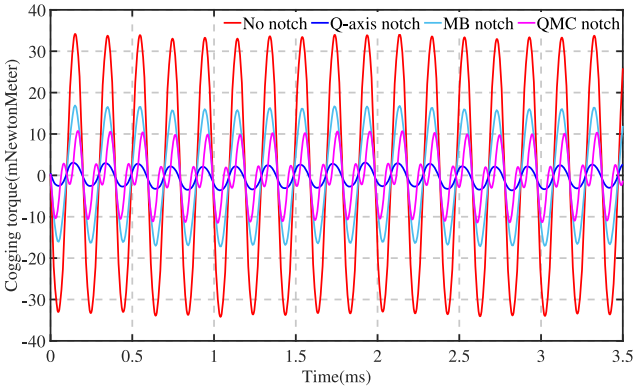

FIGURE 9. Comparison of cogging torque curves with different notch strategies.

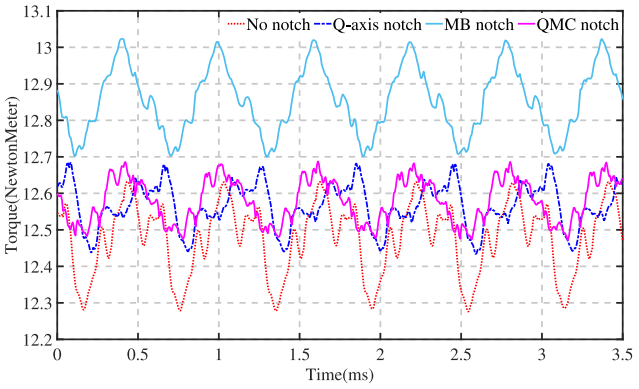

FIGURE 10. Comparison of torque curves with different notch strategies.

TABLE 5. THD analysis of back-EMF and air-gap radial flux density.

	THD of back-EMF	THD of B_r
No notch	13.14%	25.40%
Q-axis notch	13.53%	25.92%
MB notch	9.89%	21.97%
QMC notch	9.73%	20.69%

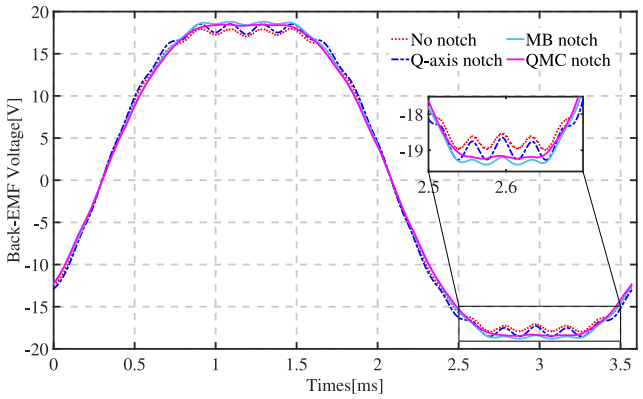

(a) No-load back-EMF

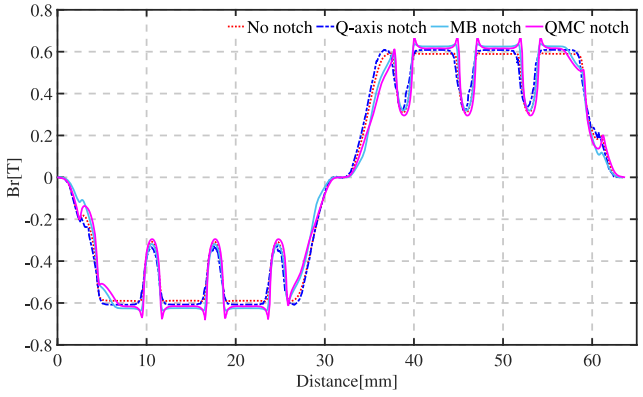

(b) Air-gap radial flux density at magnetostatic

FIGURE 11. No-load back-EMF and air-gap radial flux density at magnetostatic.

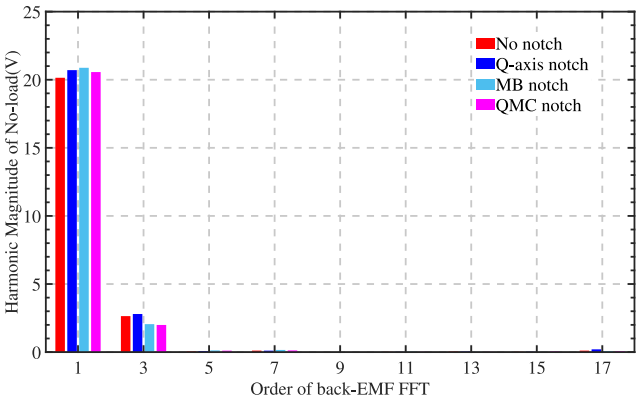

(a) Back-EMF FFT

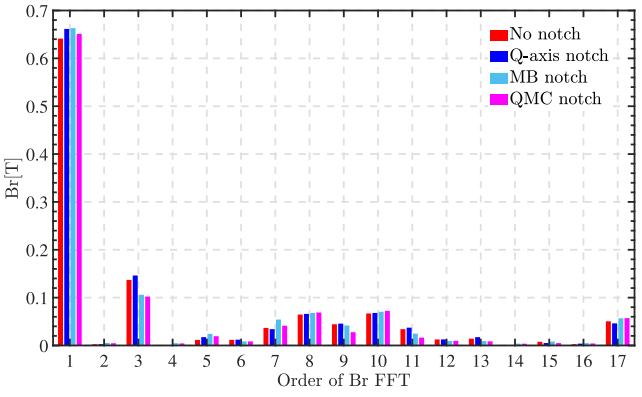

(b) Air-gap radial flux density FFT

FIGURE 12. FFT of back-EMF and air-gap radial flux density.

The radial air-gap flux density determines the magnitude of the radial electromagnetic forces in the motor, which in turn affects the motor's noise, vibration, and harshness (NVH). The harmonic content of the air-gap radial flux density can also be expressed as THD. The smaller the harmonic content, the better the sinusoidality of the air-gap flux density, and the better the NVH performance. Therefore, it is necessary to calculate the air-gap radial flux density harmonic content before and after the rotor notching of the motor to investigate whether the rotor notching increases the air-gap radial flux density harmonics. THD is calculated as follows,

$$THD = \frac{\sqrt{\sum_{k=2}^{n} (V_k)^2}}{V_1} \times 100\% \tag{11}$$

where V_n is the n-th harmonic amplitude of the air-gap flux density, and V_1 is the fundamental wave amplitude of the air-gap flux density.

Through Ansys Maxwell software analysis, the motor rotor before and after the notching of the back-EMF and radial air-gap flux density curves were obtained as shown in Fig. (11), and Fast Fourier transform (FFT) was performed to obtain the harmonic content of each order, as shown in Fig. (12), and the THD was calculated, as shown in Tab. (5).

It can be seen that the Q-axis notch design has more harmonics in the back-EMF as well as in the radial flux force than the initial design, and the other two designs have reduced the harmonic content. The increased harmonics in the back-EMF of the Q-axis notch design increase the torque ripple, but because of its smaller cogging torque, the torque ripple is also reduced by a larger amount. However, the Q-axis notch design leads to an increase in air-gap radial flux density harmonics.

V. ROTOR STRENGTH VERIFICATION

All three notching designs are near the magnetic bridge, and all of them reduce the size of the magnetic bridge, which makes the stress at the magnetic bridge more concentrated. To ensure that the mechanical structure of the motor rotor does not fail at high motor speeds after optimization of the notching design, it is necessary to verify the mechanical strength of the rotor after optimization, which means that the motor rotor strength is made to satisfy the following conditions [32],

$$\sigma \leqslant \frac{[\sigma]}{s} \tag{12}$$

where $[\sigma]$ is the allowable material stress, σ is the centrifugal stress on the rotor surface of the motor, and s is the safety factor.

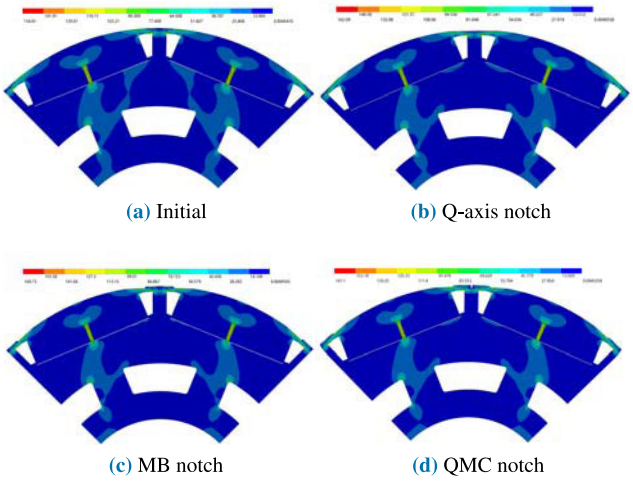

(a) Initial (b) Q-axis notch

(c) MB notch (d) QMC notch

FIGURE 13. Comparison of rotor stress analysis results.

TABLE 6. Stress comparison of different notching strategies with the initial design.

	$[\sigma]$(MPa)	σ(MPa)	s
Initial	265	154.81	1.71
Q-axis notch	265	169.73	1.56
MB notch	265	162.09	1.63
QMC notch	265	167.1	1.59

It is usually necessary to calculate the stress compliance of the rotor at the highest speed. At the same time, The performance of the material is measured at room temperature, the actual operation of the motor, especially at high speeds, the rotor surface temperature will rise to more than 100 degrees, the yield strength of the material at high temperatures will decline, so need to ensure that the safety factor greater than 1.5. The Von Mises Stress distribution is calculated by finite element software and the initial design as well as the three optimized rotor designs are compared as shown in Fig. (13). Based on the maximum stresses of the four designs and the yield strength of the material being 265 MPa, a factor of safety can be calculated for each design as shown in Tab. (6).

VI. CONCLUSION

The equations for torque ripple and cogging torque are derived. Firstly, by adjusting the pole-slot combination, the initial 6-pole/36-slot is optimized to 8-pole/36-slot, which reduces the torque ripple and cogging torque significantly. Secondly, through analysis, it is learned that cogging torque and torque ripple can be further reduced by a suitable rotor notching design, so three notching designs are devised, the Q-axis notch design, MB notch design, and QMC notch design. For each notching design, depending on the number of parameters, the optimal parameters are obtained by sweeping or numerical real-time optimization.

The research shows,

1) By choosing a suitable pole-slot combination, increasing the LCM of the pole-slot combination, and increasing the number of periods of the cogging torque, the cogging torque can be significantly reduced while the torque ripple can be significantly reduced.
2) A suitable rotor notching design can further reduce the cogging torque and torque ripple while ensuring that the average torque does not decrease or increase slightly. By notching the Q-axis and the magnetic bridge, the magnetic leakage and the air-gap density harmonic content are reduced, thus reducing the cogging torque and torque ripple.
3) All three optimized designs reduce the cogging torque and torque ripple, but the Q-axis notch design leads to an increase in the radial harmonics in the air-gap, which may affect the NVH of the motor, therefore, the other two optimized designs are recommended. The QMC notch design is recommended as the highest priority due to its ability to minimize the cogging torque as well as the air-gap radial flux density harmonics.

This paper focuses on the analysis and optimization of cogging torque and torque ripple caused by tangential electromagnetic forces in an ISG motor. In subsequent research, vibration and noise issues caused by radial electromagnetic forces will be addressed by analysing the motor's radial electromagnetic forces, structural modes, harmonic responses, and acoustical characteristics. These issues will be mitigated through further structural optimization and other measures.

REFERENCES

[1] S. Abdul Qadir, F. Ahmad, A. Mohsin A B Al-Wahedi, A. Iqbal, and A. Ali, "Navigating the complex realities of electric vehicle adoption: A comprehensive study of government strategies, policies, and incentives," *Energy Strategy Rev.*, vol. 53, May 2024, Art. no. 101379.

[2] V. K. Ramachandaramurthy, A. M. Ajmal, P. Kasinathan, K. M. Tan, J. Y. Yong, and R. Vinoth, "Social acceptance and preference of EV users—A review," *IEEE Access*, vol. 11, pp. 11956–11972, 2023.

[3] S. Jeon, G. S. Lee, D.-W. Kang, W.-H. Kim, and S. Bae, "Belt-driven integrated starter and generator using planetary gears for micro hybrid electric vehicles," *IEEE Access*, vol. 9, pp. 56201–56213, 2021.

[4] M. Cheng, L. Sun, G. Buja, and L. Song, "Advanced electrical machines and machine-based systems for electric and hybrid vehicles," *Energies*, vol. 8, no. 9, pp. 9541–9564, Sep. 2015.

[5] Y. Oh, "Design of integrated starter generator for 42v automotive electrical system," M.S. thesis, Graduate School Elect. Eng., Hanyang Univ., Seoul, South Korea, 2012.

[6] D. Wang, "Study on the electromagnetic design and control system of ISG motor for automobiles," M.S. thesis, School Electrical. Eng. Autom., Harbin Inst. Technol., Harbin, China, 2020.

[7] M.-H. Hwang, J.-H. Han, D.-H. Kim, and H.-R. Cha, "Design and analysis of rotor shapes for IPM motors in EV power traction platforms," *Energies*, vol. 11, no. 10, p. 2601, Sep. 2018.

[8] S. I. Suriano-Sánchez, M. Ponce-Silva, V. H. Olivares-Peregrino, and S. E. De León-Aldaco, "A review of torque ripple reduction design methods for radial flux PM motors," *Eng*, vol. 3, no. 4, pp. 646–661, Dec. 2022.

[9] M. S. Islam, R. Mikail, M. A. Kabir, and I. Husain, "Torque ripple and radial force minimization of fractional-slot permanent magnet machines through stator harmonic elimination," *IEEE Trans. Transport. Electrific.*, vol. 8, no. 1, pp. 1072–1084, Mar. 2022.

[10] S. M. Castano, J. W. Jiang, B. Bilgin, A. Sathyan, H. Dadkhah, and A. Emadi, "An investigation of slot-pole combinations for interior permanent magnet synchronous machines with different magnet topologies," in *Proc. IEEE Int. Electric Mach. Drives Conf. (IEMDC)*, 2017, pp. 1–8.
[11] H. Jang, H. Kim, H.-C. Liu, H.-J. Lee, and J. Lee, "Investigation on the torque ripple reduction method of a hybrid electric vehicle motor," *Energies*, vol. 14, no. 5, p. 1413, Mar. 2021.
[12] H. Ge, X. Qiu, B. Guo, J. Yang, C. Bai, and Z. Jin, "Optimized rotor shape for reducing torque ripple and electromagnetic noise," *IEEE Trans. Magn.*, vol. 58, no. 2, pp. 1–5, Feb. 2022.
[13] J.-H. Moon and D.-W. Kang, "Torque ripple and cogging torque reduction method of IPMSM using asymmetric shoe of stator and notch in stator," *J. Electr. Eng. Technol.*, vol. 17, no. 6, pp. 3465–3471, Oct. 2022.
[14] O. Ocak and M. Aydin, "An innovative semi-FEA based, variable magnet-step-skew to minimize cogging torque and torque pulsations in permanent magnet synchronous motors," *IEEE Access*, vol. 8, pp. 210775–210783, 2020.
[15] C. Peng, D. Wang, Z. Feng, and B. Wang, "A new segmented rotor to mitigate torque ripple and electromagnetic vibration of interior permanent magnet machine," *IEEE Trans. Ind. Electron.*, vol. 69, no. 2, pp. 1367–1377, Feb. 2022.
[16] L. Dai, S. Niu, W. Zhang, J. Gao, and S. Huang, "Harmonic modeling and ripple suppression of electromagnetic torque in IPMSMs," *IEEE Trans. Ind. Electron.*, pp. 1–11, 2024, doi: 10.1109/TIE.2024.3384614.
[17] T.-H. Ji, C.-H. Kim, S.-W. Jung, and S.-Y. Jung, "Design method of IPMSM using multi-objective optimization considering mechanical stress for high-speed electric vehicles," *J. Electr. Eng. Technol.*, vol. 19, no. 4, pp. 2481–2489, May 2024.
[18] M. Masoumi, A. Tsao, C. Abeyrathne, A. Sahu, and B. Bilgin, "Investigation of the impact of rotor shaping on the torque and radial force harmonics of a V-shape interior permanent magnet synchronous machine," *IET Electric Power Appl.*, vol. 18, no. 2, pp. 185–194, Feb. 2024.
[19] H. Li, "Research on mechanism and optimization of cogging torque and torque ripple of embedded permanent magnet synchronous motor," M.S. thesis, School Elect.. Eng. Autom., Nanjing Normal Univ., Nanjing, China, 2018.
[20] M.-H. Hwang, H.-S. Lee, and H.-R. Cha, "Analysis of torque ripple and cogging torque reduction in electric vehicle traction platform applying rotor notched design," *Energies*, vol. 11, no. 11, p. 3053, Nov. 2018.
[21] X. Wan, S. Yang, Y. Li, Y. Shi, and J. Lou, "Minimization of cogging torque for V-type IPMSM by the asymmetric auxiliary slots on the rotor," *IEEE Access*, vol. 10, pp. 89428–89436, 2022.
[22] K. Sun and S. Tian, "Multiobjective optimization of IPMSM with FSCW applying rotor notch design for torque performance improvement," *IEEE Trans. Magn.*, vol. 58, no. 5, pp. 1–9, May 2022.
[23] S. He, P. Zhang, M. Muir, and B. Koch, "Rotor optimization to reduce electric motor noise," *SAE Int. J. Adv. Curr. Prac. Mobility*, vol. 6, no. 2023-01-0540, pp. 39-47, 2023, doi: 10.4271/2023-01-0540.
[24] R. Thike and P. Pillay, "Mathematical model of an interior PMSM with aligned magnet and reluctance torques," *IEEE Trans. Transport. Electrific.*, vol. 6, no. 2, pp. 647–658, Jun. 2020.
[25] J. Zou and Y. Xu, *Analysis and Suppression of Electromagnetic Vibration of Permanent Magnet Synchronous Machine*, 1st ed., S. Xiong, Ed., Arlington, VA, USA: National Defense Industry Press, Jan. 2023.
[26] M. S. Rafaq, W. Midgley, and T. Steffen, "A review of the state of the art of torque ripple minimization techniques for permanent magnet synchronous motors," *IEEE Trans. Ind. Informat.*, vol. 20, no. 1, pp. 1019–1031, Jan. 2024, doi: 10.1109/TII.2023.3272689.
[27] Z. Zhang, W. Hua, P. Wang, W. Yu, M. Hu, G. Zhang, and M. Cheng, "Torque characteristics of SPM-FS machines with functional-contour salient pole rotors considering manufacturing error," *IEEE Trans. Energy Convers.*, vol. 37, no. 4, pp. 2645–2656, Dec. 2022.
[28] S.-M. Hwang, J.-B. Eom, G.-B. Hwang, W.-B. Jeong, and Y.-H. Jung, "Cogging torque and acoustic noise reduction in permanent magnet motors by teeth pairing," *IEEE Trans. Magn.*, vol. 36, no. 5, pp. 3144–3146, Sep. 2000.
[29] X. Sun, Z. Shi, G. Lei, Y. Guo, and J. Zhu, "Multi-objective design optimization of an IPMSM based on multilevel strategy," *IEEE Trans. Ind. Electron.*, vol. 68, no. 1, pp. 139–148, Jan. 2021.
[30] M. Abdel-Basset, L. Abdel-Fatah, and A. K. Sangaiah, "Chapter 10—Metaheuristic algorithms: A comprehensive review," in *Computational Intelligence for Multimedia Big Data on the Cloud With Engineering Applications* (Intelligent Data-Centric Systems), A. K. Sangaiah, M. Sheng, and Z. Zhang, Eds., New York, NY, USA: Academic, 2018, pp. 185–231.
[31] S. Verma, M. Pant, and V. Snasel, "A comprehensive review on NSGA-II for multi-objective combinatorial optimization problems," *IEEE Access*, vol. 9, pp. 57757–57791, 2021.
[32] M.-J. Jeong, K.-B. Lee, H.-J. Pyo, D.-W. Nam, and W.-H. Kim, "A study on the shape of the rotor to improve the performance of the spoke-type permanent magnet synchronous motor," *Energies*, vol. 14, no. 13, p. 3758, Jun. 2021.

YUNFEI DAI received the B.S. degree in aeronautical mechanical engineering from the Air Force First Aeronautical College, in 2006, and the M.S. degree in mechatronic engineering from Huazhong University of Science and Technology, in 2013. He is currently pursuing the Ph.D. degree in electronic engineering with Cheongju University.

His research interests include design and optimization of electric machines and multi-physics field problems.

DONG-WOO LEE (Member, IEEE) was born in South Korea, in 1977. He received the B.S. and M.S. degrees in mechatronics from Korea University, South Korea, in 2004 and 2008, respectively, and the Ph.D. degree in functional control systems from Shibaura Institute of Technology, Tokyo, Japan, in 2019. From 2008 to 2021, he was with the Electric Vehicle Research and Development Laboratory, LG Electronics (LGE), Seoul, South Korea, as a Senior Research Engineer. At LGE, he developed a traction motor and inverter systems for electric vehicles. From 2021 to 2023, he was a Senior Research Engineer with the Inverter Development Division, LG Magna e-Powertrain, Incheon, South Korea. Since October 2023, he has been an Assistant Professor with the Department of Electrical Engineering, Cheongju University. His research interests include electric machine drives, power conversion, and fault detection in electric vehicle applications.

HOUNG-KUN JOUNG was born in Cheongju, Chungcheongbuk-do, South Korea, in 1977. He received the B.S. degree from the Department of Electrical Engineering, Semyung University, in 2002, and the M.S. and Ph.D. degrees from the Department of Electrical Engineering, Hanyang University, in 2004 and 2017, respectively. From 2011 to 2017, he was an Assistant Professor with Korea Polytechnic College. He has been an Assistant Professor with the Department of Electrical Engineering, Cheongju University, since 2019. He has authored ten journal articles and has one patent. His current research interests include control systems, motor control systems, smart factory systems, and collaborative robot.

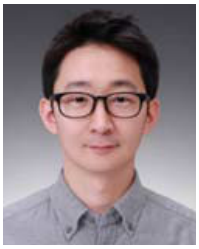

HO-JOON LEE (Member, IEEE) received the B.S., M.S., and Ph.D. degrees in electrical engineering from Hanyang University, Seoul, South Korea, in 2009, 2011, and 2015, respectively.

He joined Cheongju University, in 2020, where he is currently a Professor with the Department of Electrical and Control Engineering. His research interests include electrical machinery design, electro-magnetic field analysis, and its drive and testing, such as electric vehicles and electrification systems.